Friction

Research Article

When ultrathin carbon layer system chemistry dictates the tribo-interface: Origin of slippery and wear-resistant surfaces

Rajesh Kumar[1,2], Pankaj Bharti[1,2], Reuben J. Yeo[3], Avanish K. Srivastava[1,2], Chetna Dhand[1,2,✉], Neeraj Dwivedi[1,2,✉]

Cite this article: Kumar R, Bharti P, Yeo RJ, et al. *Friction* 2025, **13**(9): 9441061. https://doi.org/10.26599/FRICT.2025.9441061

ABSTRACT: Overcoats are predominantly employed to tackle tribological challenges in numerous moving mechanical systems. However, when overcoats are thinned down to sub-10 nm levels, their performance gets significantly compromised because of the dominance of surface and interface effects. Here, we discovered the efficacy of the chemistry of sub-10 nm thick carbon-based overcoats in regulating the friction and wear of rough ceramic surfaces, particularly those of Al_2O_3+TiC (AlTiC). Carbon overcoats up to 4 nm in thickness grown with low-energy (~4–5 eV) atoms/ions caused no significant changes in the tribological performance of AlTiC. However, carbon overcoats grown at a moderate energy of 90 eV experienced an exceptional reduction in friction and wear of AlTiC at similar thickness levels up to 4 nm. The addition of a 6 nm thick RF-sputtered carbon layer on top of these carbon overcoats caused no significant improvement in the tribological performance. However, the addition of a multilayer graphene overlayer was found to slightly reduce the friction further for the thicker carbon overcoats grown at 90 eV. Chemical bonding and carbon microstructural analyses, along with ion interaction simulations, were performed to elucidate the fundamental mechanisms behind the observed friction and wear performances. We discovered that the atomic mixing and high sp^3 bonding caused by the 90 eV growth process primarily dictated the friction and wear control at ⩽ 10 nm overcoat thicknesses. Thus, by adopting suitable carbon overcoat technology, excellent tribological properties can be attained even at sub-5 nm overcoat thickness levels, which is critical for numerous applications.

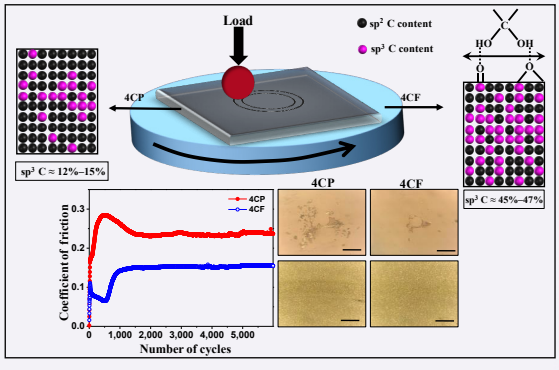

KEYWORDS: ultrathin overcoats; ceramic; tribology; friction and wear; carbon coatings

1 Introduction

In moving mechanical systems containing sliding components, the energy required to slide the components over one another strongly depends on the frictional forces between the two sliding surfaces. High frictional forces and hence high coefficients of friction (COFs) consequently lead to a substantial amount of energy that is wasted just to overcome friction in moving machine assemblies [1–4]. Moreover, high friction also promotes wear damage to the components and causes premature failure of the systems [5, 6]. Approximately 20% of energy is used to overcome friction and wear challenges worldwide [7–9]. Thus, controlling friction and wear is of great technological interest.

Friction and wear severely affect high-precision technologies such as micro-/nano-electromechanical systems (MEMS/NEMS) [10–12], magnetic media and read/write heads of hard disk drives (HDDs) [13–15] and magnetic tape drives (MTDs) [16–19], probe tips for atomic force microscopy (AFM) in tapping or contact mode [20–22], micro-gears [23, 24], micro-/nano-resonators [25], etc. MTD is one of the oldest magnetic recording technologies for archival data storage that is still being used today for this purpose because of its overall affordability per byte, ease of storage, minimal power consumption, large storage capacity, and long-term durability in data retention [26, 27]. With growing dependence on digital information in daily life and greater reliance on cloud storage, a steady rise in demand for MTDs is anticipated in the near future [28, 29]. A forecast by the "International Magnetic Tape Storage Roadmap" predicts that the areal density of tape storage will reach 91 gigabits per square inch of tape media by 2025, and this value is expected to exceed 200 gigabits per square inch by 2028 [29, 30].

[1] CSIR-Advanced Materials and Processes Research Institute (AMPRI), Bhopal 462026, India. [2] Academy of Scientific and Innovative Research (AcSIR), Ghaziabad 201002, India. [3] Institute of Materials Research and Engineering (IMRE), Agency for Science, Technology and Research (A*STAR), 2 Fusionopolis Way, Innovis #08-03, Singapore 138634, Singapore.

✉ Corresponding authors. E-mail: N. Dwivedi, neerajdwivedi6@gmail.com, neeraj.dwivedi@ampri.res.in; C. Dhand, chetnachem24@gmail.com, chetna.dhand@ampri.res.in

Received: May 30, 2024; Revised: October 23, 2024; Accepted: December 15, 2024

However, a longstanding concern that persists with MTDs is the substantial wear of Al_2O_3+TiC (AlTiC) ceramics [31] and "pole tip recession (PTR)" [17, 32], a phenomenon that represents a gradual erosion of the read/write head's magnetic poles, leading to increased magnetic spacing. While considerable stress has been placed on finding solutions for PTR over the years, relatively less attention has been given to developing effective strategies to tackle the wear concerns of AlTiC ceramics. Owing to the dual-phase nature of AlTiC composite material, the wear of AlTiC would preferentially generate hard TiC debris that gets trapped between the sliding interface of the tape media and read/write head, thereby further aggravating the wear conditions. Thus, controlling the friction and wear of AlTiC is also highly important for wear-durable and sustainable data storage technologies. Furthermore, wear significantly influences the performance and reliability of MTD in terms of storage capacity, power consumption, and longevity. Wear can lead to surface degradation of the tape media and the read/write head, resulting in data loss or errors during read/write operations [33]. The degradation of both the tape media and the read/write heads due to wear shortens the lifespan of these critical components and reduces the overall longevity of the device. Eventually, the need for frequent replacement or maintenance increases the cost of power consumption for manufacturing of more devices.

Protective overcoats remain a primary choice for controlling the tribological challenges in various moving mechanical systems, including MTDs [34, 35]. For example, Sourty et al. [36] demonstrated that 20–40 nm chromium oxide coatings improve the wear resistance of magnetic tape heads. Bernhard et al. [37] studied sub-10 nm overcoats for AlTiC ceramic surfaces. Matlak et al. [38] explored ultrathin protective coatings for heat-assisted magnetic recording media. Ebrahimi et al. [39] investigated the nanoscale friction and wear behavior of amorphous carbon for hard-disk drives. Mangolini et al. [40] suggested that silicon- and oxygen-containing ultrathin hydrogenated amorphous carbon films were promising for several applications because of their high thermal stability and low residual stress. However, owing to the rigorous and complex tribo-interface in MTDs as well as the constraint to keep the thickness of the overcoat as low as possible to maintain a small magnetic spacing, many overcoats that have been studied for MTDs face challenges in terms of their wear durability, leading to their premature failure. As the demand for data storage continues to grow, the need for higher data storage densities is also becoming more pressing. This has led to more research efforts aimed at using ultrathin overcoats with reduced thicknesses while maintaining exceptional wear protection. Sub-10 nm overcoats hold great potential for future high-storage-density MTDs. Recently, significant contributions have been made by Rismani et al. [41], Yeo et al. [17], and Dwivedi et al. [5] towards understanding the wear protection capabilities and fundamental mechanisms of sub-10 carbon-based films. However, enhancing the friction and wear control properties of these sub-10 nm overcoats through innovative methods continues to be a pivotal focus in materials research.

Motivated by the importance of developing innovative designs for ultrathin wear-protective overcoats, in this work, we studied a range of ⩽ 10 nm high-performance monolithic and hybrid carbon overcoats for AlTiC, which can also be extended to other ceramic surfaces. The tribological performances of these monolithic and hybrid overcoats were compared, and the underlying mechanisms were elucidated with the help of relevant characterization techniques to probe the chemical bonding, carbon microstructure, and extent of atomic mixing, aided by ion interaction simulations.

2 Experimental methods

The details of the samples used in this work, together with their respective nomenclature, are provided in Table 1. The first series of carbon overcoats with thicknesses of 1, 3, and 4 nm were deposited on flat ceramic AlTiC substrates using pulsed direct current (DC) magnetron sputtering (energy of atoms/ions of approximately 4–5 eV) at a working pressure of 5 mTorr, Ar flow rate of 20 standard cubic centimeters per minute (sccm), and applied power of 100 W. These pulsed DC-sputtered carbon films were labelled as 1CP, 3CP, and 4CP, respectively, corresponding to different carbon thicknesses [42]. The second series of carbon overcoats with thicknesses of 1, 3, and 4 nm were deposited on flat ceramic AlTiC substrates using an energetic ion deposition process (viz. filtered cathodic vacuum arc (FCVA)) at a carbon ion energy of 90 eV, and the resulting samples were labeled as 1CF, 3CF, and 4CF, respectively [42]. Bare AlTiC (labelled simply as AlTiC) was included as a reference. To fabricate hybrid carbon overcoats, a few more series of samples were prepared by employing two different types of carbon. The third series of samples comprise all the CP and CF series samples with the addition of a 6 nm thick radio frequency (RF, 13.56 MHz) magnetron-sputtered carbon layer (6C) atop. The 6C films were grown at a working pressure of 0.009 mbar, an Ar flow rate of 18 sccm, and an RF power of 90 W. The fourth series of samples comprise all the CP and CF series samples with multilayer graphene (G) (thickness ~6–8 nm) atop. The G solution was prepared in isopropyl alcohol (IPA) at a concentration of 5 mg/mL. Subsequently, the G coatings were applied to the CP and CF samples by spin coating [43, 44].

After overcoat fabrication, the thickness, chemical bonding, structure, and tribological properties of the films were characterized. High-resolution transmission electron microscopy (HRTEM) was used to measure and verify the thicknesses of the overcoats. For thickness measurements using HRTEM, the same coatings were deposited on Si substrates and used for characterization due to the ease of thinning down and polishing the Si substrate during HRTEM sample preparation compared with the AlTiC ceramic substrate. The coatings applied on the AlTiC ceramic substrate were used for tribological testing and other characterizations. Tribological measurements were conducted using a low-load tribometer (Ducom Instruments, India) in a ball-on-disk configuration using a rotary drive. A sapphire (Al_2O_3) ball with a diameter of 2.0±0.1 mm was employed as the counter-face material. The experiments were conducted at a controlled temperature of 25±1 °C, a relative humidity of 40%±5%, a sliding speed of 100 r/min (or a 1.05 cm/s linear speed), and a normal load of 1 N. Each tribological test comprised a total of 6,000 cycles (revolutions) corresponding to a sliding distance of 3,768.0 cm. After each tribological test, we examined the ball and wear track damage to the sample with an optical microscope. The surface roughness and morphology/topography were investigated using atomic force microscopy (AFM) on a Nanosurf CoreAFM apparatus (Switzerland). A Dyn190Al tip/cantilever (Nanosurf) attached to the Nanosurf CoreAFM was scanned over an area of 10 μm × 10 μm in the tapping mode configuration to acquire the images. X-ray photoelectron spectroscopy (XPS) measurements were performed on a VG ESCALAB 220I-XL instrument (Thermo Fisher Scientific, USA) using a monochromatic Al Kα source (1,486.6 eV). XPS measurements were conducted under ultrahigh vacuum with a base pressure of ~10^{-9} Torr. The spot size of the X-ray beam on the sample was kept at 200 μm × 200 μm. A pass energy of 55 eV and a step size of 0.1 eV were used for the high-resolution scans.

Table 1 List of different samples used in this work with detailed descriptions

Sample label	Sample description	Sample schematic
Bare AlTiC	Pristine Al_2O_3+TiC containing 70% Al_2O_3 and 30% TiC.	
1CP	AlTiC substrate with a 1 nm thick carbon overcoat grown at 4 eV using pulsed DC sputtering.	
3CP	AlTiC substrate with a 3 nm thick carbon overcoat grown at 4 eV using pulsed DC sputtering. The thickness of carbon measured by HRTEM was 3.3±0.3 nm.	
4CP	AlTiC substrate with a 4 nm thick carbon overcoat grown at 4 eV using pulsed DC sputtering. The thickness of carbon measured by HRTEM was 4.4±0.3 nm.	
1CF	AlTiC substrate with a 1 nm thick carbon overcoat grown at 90 eV using energetic vacuum arc process.	
3CF	AlTiC substrate with a 3 nm thick carbon overcoat grown at 90 eV using energetic vacuum arc process. The thickness of carbon measured by HRTEM was 3.0±0.1 nm.	
4CF	AlTiC substrate with a 4 nm thick carbon overcoat grown at 90 eV using energetic vacuum arc process. The thickness of carbon measured by HRTEM was 4.1±0.1 nm.	
6C-AlTiC	AlTiC with ~6 nm thick carbon layer atop deposited using RF sputtering.	
6C-1CP	1CP with ~6 nm thick carbon layer atop deposited using RF sputtering.	
6C-3CP	3CP with ~6 nm thick carbon layer atop deposited using RF sputtering.	
6C-4CP	4CP with ~6 nm thick carbon layer atop deposited using RF sputtering.	
6C-1CF	1CF with ~6 nm thick carbon layer atop deposited using RF sputtering.	
6C-3CF	3CF with ~6 nm thick carbon layer atop deposited using RF sputtering.	
6C-4CF	4CF with ~6 nm thick carbon layer atop deposited using RF sputtering.	
G-AlTiC	AlTiC with a multilayer graphene atop.	
G-1CP	1CP with a multilayer graphene atop.	
G-3CP	3CP with a multilayer graphene atop.	
G-4CP	4CP with a multilayer graphene atop.	
G-1CF	1CF with a multilayer graphene atop.	
G-3CF	3CF with a multilayer graphene atop.	
G-4CF	4CF with a multilayer graphene atop.	

Color legend: purple = CP, orange = CF, light blue = 6C, and grey = G.

UV Raman measurements of the samples were carried out using a Jobin Yvon LABRAM-HR Raman spectrophotometer (France). An excitation wavelength of 325 nm from a He–Cd laser was used for the UV Raman measurements. The laser spot size was fixed at 1 μm for Raman analysis.

3 Results and discussion

The thicknesses of the overcoats were measured using HRTEM, as shown in Figs. 1(a)–1(d). The thicknesses of carbon layers were found to be ~3.3, ~4.4, ~3, and ~4.1 nm in samples 3CP, 4CP, 3CF, and 4CF, respectively, which were close to the intended thicknesses of the overcoats. We examined the topography and roughness of the bare, CP series (1CP, 3CP, and 4CP), and CF series (1CF, 3CF, and 4CF) samples (Section S1 in the Electronic Supplementary Material (ESM) for details). The AFM images (Fig. S1 in the ESM) revealed similar morphologies for all the samples that were representative of the AlTiC substrate, viz. TiC particles embedded in an Al_2O_3 matrix. The root-mean-square (RMS) roughness was computed over a 10 μm × 10 μm area (see Table S1 in the ESM for details). The RMS roughness of bare AlTiC was found to be 6–11 nm, while the RMS roughnesses of the CP and CF series samples were also found to be in the range

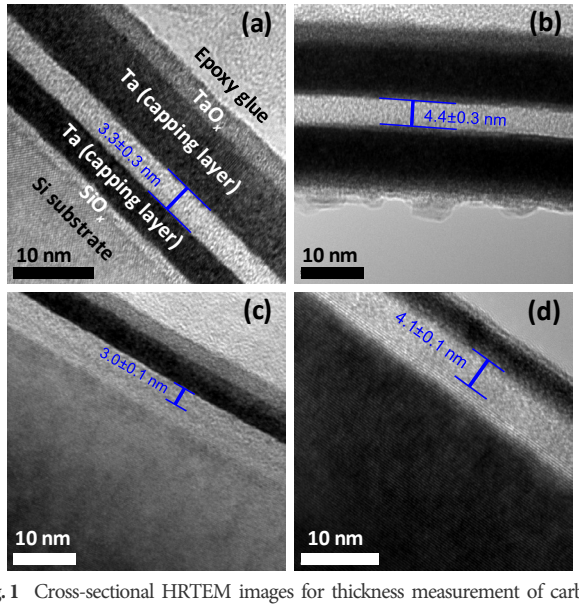

Fig. 1 Cross-sectional HRTEM images for thickness measurement of carbon layer in samples (a) 3CP, (b) 4CP, (c) 3CF, and (d) 4CF. To obtain good contrast and clearly measure the carbon layer thickness using HRTEM, a tantalum capping layer was intentionally grown on top of the carbon layers.

of 7.6–11.8 nm, similar to that of bare AlTiC. This indicated that the roughness of the coated samples did not significantly change after carbon layer deposition.

Next, we focused on the friction (Figs. 2(a) and 2(b)) and wear (Fig. 3) properties of the different carbon overcoats on AlTiC. Bare AlTiC showed COFs around ~0.25–0.26, and a visible wear track was observed on the sample, with some wear debris transferred to the ball (Fig. 3). To alter the friction and wear of AlTiC, various carbon overcoats were applied. While the application of pulsed DC-sputtered carbon overcoats (1CP, 3CP, and 4CP) negligibly altered the COF of AlTiC regardless of the overcoating thickness of 1–4 nm (Figs. 2(a) and 2(b)), these overcoats certainly reduced the degree of wear, as confirmed by the observation of relatively fainter wear tracks in the CP series samples than in the bare AlTiC samples (Fig. 3). Moreover, the CF series samples demonstrated excellent friction control (Figs. 2(a) and 2(b)), with the lowest COF of ~0.17 attained for 4CF, which was a ~40% reduction in friction with respect to that of bare AlTiC. This performance is impressive considering that the thickness of the carbon overcoat in 4CF is just 4 nm and that the tribo-contacts in these systems are quite rough. Moreover, the CF series samples with thicknesses of 3 and 4 nm attained COFs as low as ~0.07 (lower than 0.1) for the first few hundred frictional cycles (up to 500 cycles) (Fig. 2(a)), demonstrating their ability to produce highly lubricating surfaces. The same trend was observed for their wear properties, where the CF series samples presented many fainter wear tracks, especially those with 3 and 4 nm thicknesses (Fig. 3), suggesting the excellent wear resistance and wear durability of these coatings. Thus, the carbon coatings grown with 90 eV ion energy were highly effective in addressing the friction and wear concerns of rough AlTiC surfaces. This work revealed that the wear durability of these overcoats could still be observed at even lower thicknesses of 3–4 nm, which is an outstanding achievement from the viewpoints of increasing the storage capacity and durability of magnetic data storage devices.

When an additional RF-sputtered carbon layer (6C) was applied on top of the CP and CF series samples, generally no further improvement in friction and wear control was observed. Conversely, the additional 6C layer degraded the tribological performance of the CF series samples, as indicated by the increased COF in the 6C-CP series samples (Figs. 2(a) and 2(b)). Thus, these results suggested that the addition of a 6 nm thick RF-sputtered carbon coating was disadvantageous for friction performance. Furthermore, although the application of a multilayer graphene coating (G) did not contribute to improving the tribological contact of 1CP and 3CP (Figs. 2(a), 2(b), and 3), it certainly reduced the friction on 4CP while maintaining/slightly improving the wear resistance. Therefore, the combination of a higher pulsed DC carbon thickness (4 nm) capped with multilayer graphene works in a synergistic way to boost the tribological performance. Similarly, the addition of the G coating did not significantly influence the tribological behavior of the CF series samples, even though sample G-3CF showed relatively lower friction than 3CF (Figs. 2(a) and 2(b)). Overall, the crucial finding of this work is that standalone carbon coatings grown at 90 eV (CF series samples) by themselves exhibit outstanding lubricating and wear resistance properties, even at extremely low overcoat thicknesses of 1–4 nm, and do not actually require additional sputtered carbon or multilayer graphene overlayers to further alter their tribological contacts.

To gain insight into the friction and wear mechanisms, it is crucial to understand the bonding environment (Figs. 4(a) and 4(f)) and carbon microstructure (Figs. 4(b)–4(e)) within the carbon layer. Figure 4(a) shows the deconvoluted XPS C 1s spectra of CP and CF series samples, where all the samples reveal sp^2 C, sp^3 C, and various bonding states of carbon with oxygen [42]. By using a method of peak area ratio, the sp^3 bonding contents of these samples were estimated (Fig. 4(f)). Figures 4(b) and 4(c) show the visible and UV Raman spectra of these samples. The spectra clearly reveal the characteristic G peak of carbon along with the D peak corresponding to disorder [42, 45]. The presence of the G peak arises from the E_{2g} bond stretching motion involving a pair of sp^2-bonded carbon atoms. On the other hand, the D peak is linked to the existence of ring-like sp^2-bonded structures in the carbon network. After peak fitting, the G peak positions (Fig. 4(d)) and the intensity ratios of the D to G peak (I_D/I_G) (Fig. 4(e)) were also estimated. Following Dwivedi's 3-phase model for ultrathin carbon films [42] and Ferrari and Robertson's 3-stage model [45], the sp^3 bonding contents of these coatings were estimated based on the extent of the G peak shift in UV Raman spectra (Fig. 4(f)). Sample 1CP showed sp^3 bonding content of approximately 5%–7%, which increased to a maximum of approximately 14%–15% for the 4 nm thick sputtered carbon film (4CP). On the other hand, while the 90 eV-grown 1 nm thick carbon (1CF) showed sp^3 bonding of approximately 9%–10%, the sp^3 bonding content was drastically increased to approximately 45% for the 3 nm thick film (3CF) and approximately 50% for the 4 nm thick film (4CF). This suggests that energetic carbon deposition promotes sp^3 bonding. Additionally, unlike the sputtered carbon in the CP series samples, the I_D/I_G ratios in the CF series samples were negligible, suggesting that the sp^3-rich carbon matrix contained less sp^2 disorder or fewer sp^2 crystallites.

Transport of ions in matter (TRIM) simulations were performed to obtain further insight into this phenomenon. TRIM is a Monte Carlo-based simulation program that was employed to understand the interaction of incoming ions/atoms impinging onto various host materials. In this case, we studied the interactions of 4 and 90 eV carbon ions with the Al_2O_3+TiC (or AlTiC) host matrix to understand the atomic mixing and interfacial strength of the coatings. The interaction between the carbon atoms/ions and substrate is illustrated in Figs. 5(a) and 5(b). When 4 eV energy carbon atoms/ions (mimicking the carbon energy of the sputtered CP series samples) were projected onto the AlTiC matrix (Fig. 5(a)), they interacted only with the very top region of the substrate and caused minimal atomic mixing. In contrast, when 90 eV carbon atoms/ions were projected onto the AlTiC substrate, the carbon atoms could propagate deeper inside the matrix and cause significant atomic mixing. This is demonstrated in Movie S1 in the ESM. The different carbon–substrate interactions can also be visualized with the help of the ball models shown in Figs. 5(a) and 5(b). Thus, the interfacial adhesion, strength, and interfacial robustness are expected to be significantly greater for the CF series samples than for the CP series samples. Additionally, owing to the highly energetic carbon in the CF series samples, the carbon atoms/ions that penetrate the growing carbon layer, grow sub-surface and densify the carbon network, resulting in a higher sp^3 carbon content, in contrast to the less energetic carbon atoms/ions (4 eV) in the CP series samples.

We now discuss the mechanisms governing friction and wear in various tribo-pairs. The Al_2O_3–AlTiC tribosystem represents a ceramics–ceramics contact, and the lattice structures of the two materials closely align, resulting in commensurate contacts. Consequently, this interaction results in a moderate level of friction. Since the mechanical properties of both materials are similar, not much wear was observed. Carbon, a mixed network of sp^2 and sp^3 bonding, is known to induce lubricity. The sp^2-bonded graphitic carbon exhibits low friction owing to its low shear

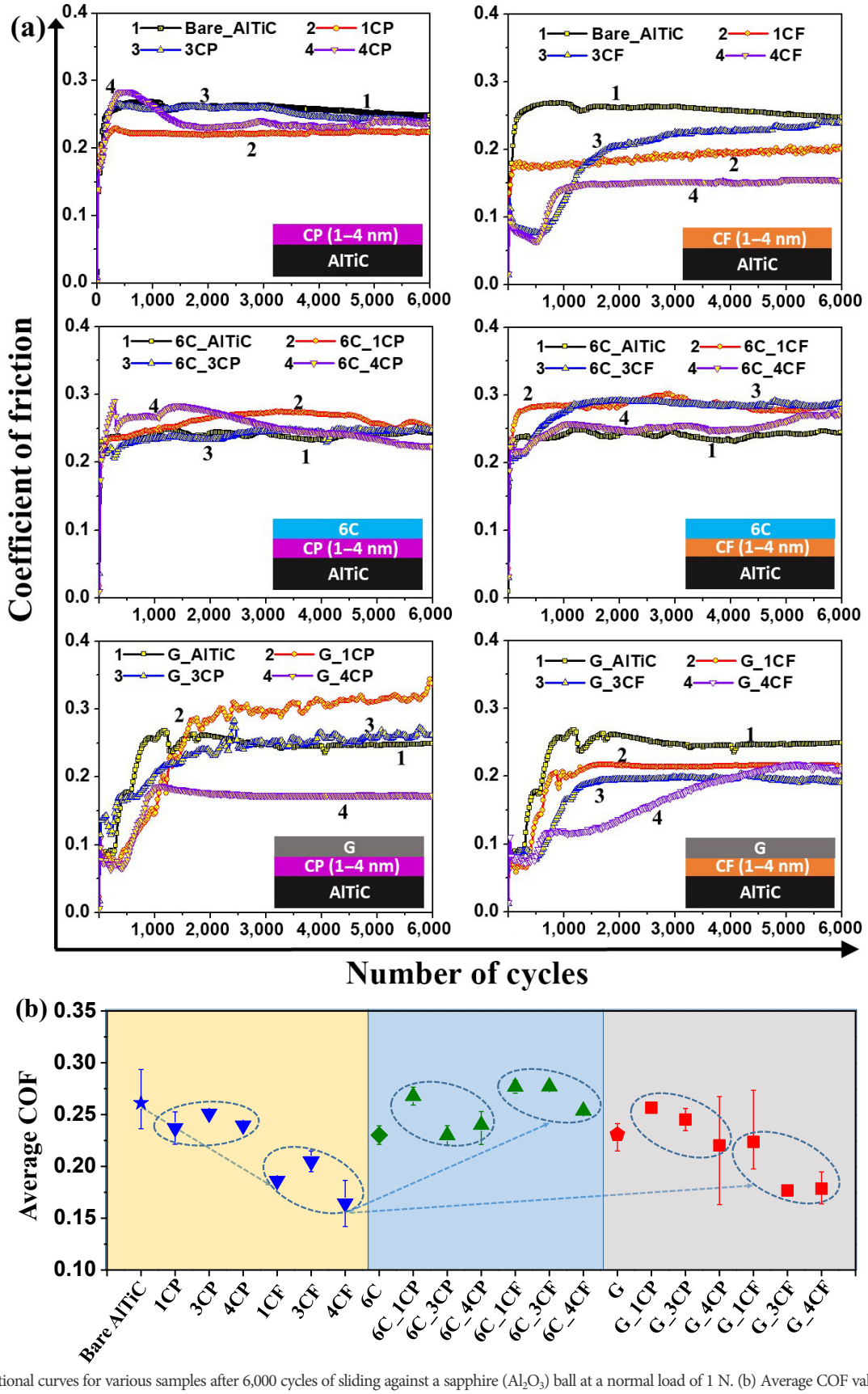

Fig. 2 (a) Frictional curves for various samples after 6,000 cycles of sliding against a sapphire (Al_2O_3) ball at a normal load of 1 N. (b) Average COF values (computed over entire 6,000 cycles) are based on two to three measurements on each sample to obtain a more accurate representation of their friction and wear characteristics. Circles represent average COFs of many CF or CP series samples with different overcoat thicknesses. The subsequent arrows represent how the COF first largely decreases with increasing thickness of CF layer from 1 to 4 nm, followed by a general increase in average COF through introduction of either a 6C layer or a G layer on CF series samples.

清華大学出版社 Tsinghua University Press | SciOpen

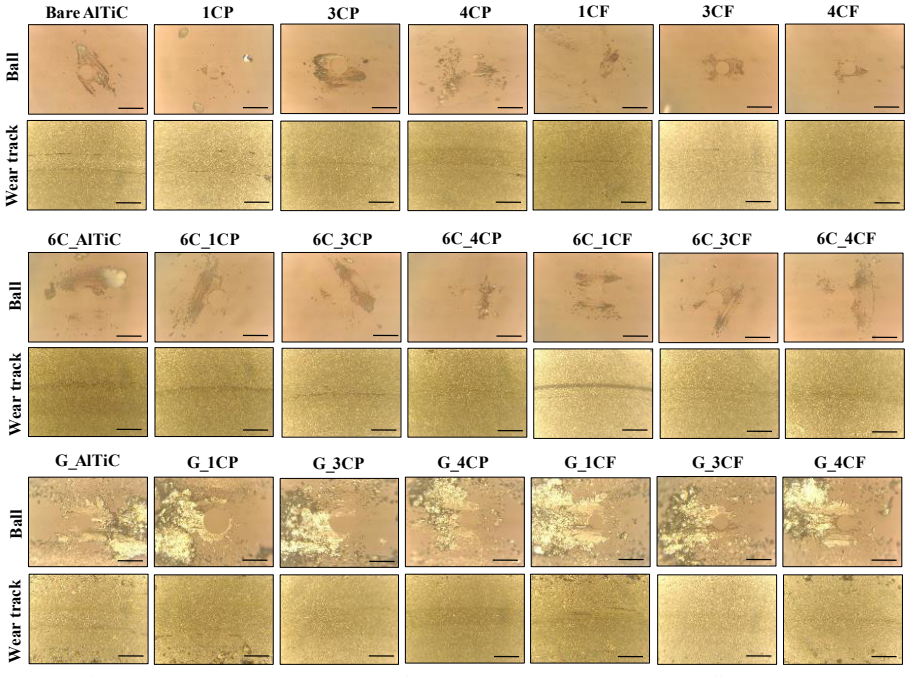

Fig. 3 Optical microscope images of balls (top) and wear tracks (bottom) after ball-on-disk tribological tests on different samples subjected to 6,000 cycles of sliding. Scale bars in the optical microscope images represent 100 μm.

strength [46, 47], while the sp^3-bonded diamond or tetrahedral carbon induces lubricity under specific conditions, such as in humid environments, due to the passivation of dangling bonds by hydrogen or hydroxyl groups through the dissociation of water, thereby effectively mitigating the friction and wear [48]. Additionally, sp^3-bonded carbon contributes to the hardness and rigidity and hence the wear resistance of the material. When monolithic carbon coatings from the CP series were introduced onto AlTiC, surprisingly, no measurable change in friction was observed compared with that of the bare AlTiC. Initially, we did not expect that a 1–4 nm thick carbon coating would be sufficient to modify such a rough tribo-contact. However, when monolithic carbon coatings from the CF series with thicknesses of 1–4 nm were introduced, the COF significantly reduced by approximately 40% (in sample 4CF) compared with that of bare AlTiC. Through tribological ball-on-disk tests, we observed that in the ultrathin regime (1–4 nm thickness), the friction of the low-sp^3-bonded carbon films (CP series) did not decrease as the carbon layer thickness increased from 1 to 4 nm. In contrast, the relatively high amount of sp^3-bonded carbon films (CF series) had a more pronounced effect on reducing the friction with increasing film thickness from 1 to 4 nm. Furthermore, the CF and CP series samples differ from each other only in terms of the sp^3 bonding content and the extent of atomic mixing, since the overcoat thicknesses are similar in these two series of samples. These findings confirm that sp^3 bonding and atomic mixing are the dominant factors in carbon coatings to control the friction and wear of ceramic surfaces. The atomic mixing strengthens the interface and interaction of the film with the substrate. Likewise, enhanced resistance against wear due to high sp^3 bonding does not significantly alter the contact area, and at the same time passivation of the sp^3-bonded surface by functional moieties from humid conditions facilitates contact sliding through the detachment and re-attachment of these functional groups to the surface. Together, these factors synergistically contribute to reducing the friction of the CF series samples.

Following the same logic, it is likely that the application of the 6C overlayer did not further reduce the friction and wear of the CP series samples because of its negligible effect on the sp^3 bonding and atomic mixing of CP series samples. Instead, it led to a worsening of the tribological properties of the CF series samples. The 6C layer was deposited by the RF sputtering process, which is expected to involve more sp^2 bonding (or less sp^3 bonding), similar to what was observed for the CP series samples. Thus, the application of the 6C coating on the CF series samples, especially for 3–4 nm thick CF carbon, results in the formation of a soft (6C) on the hard (3CF or 4CF) layered carbon structure. Consequently, during the tribological ball-on-disk measurement, wear is initiated on the relatively softer 6C layer, leading to the observation of more wear debris in the 6C-CF series samples than in the CF series samples. This finding further emphasizes that high sp^3 bonding and interfacial robustness are more crucial factors than the overall carbon coating thickness in achieving lubricating and wear-resistant surfaces. Furthermore, the application of a multilayer graphene overlayer was also found to reduce the friction of the CP and CF series samples with greater carbon layer thicknesses (3–4 nm). This is attributed to the pure sp^2 carbon-bonded network in graphene, which reduces the shear strength and promotes the ease of sliding across the graphene layers.

Finally, we present a ball model for the 4CP and 4CF samples to illustrate the sp^2 and sp^3 bonding contents and their correlation with the observed friction and wear behavior. In this model, the black balls represent the sp^2 content, while the purple balls represent the sp^3 content in ultrathin carbon overcoats. In the 4CF sample, low friction arises from the passivation of surface dangling bonds under highly humid conditions, along with some contribution from sp^2 bonding either present in the material and/or generated as a consequence of contact sliding. The passivation of surface dangling bonds leads to a less reactive surface. Likewise, high sp^3 bonding and a greater degree of atomic mixing between the carbon overcoat and the substrate contribute to better wear resistance in 4CF than in 4CP.

4 Conclusions

In summary, we have demonstrated that monolithic carbon

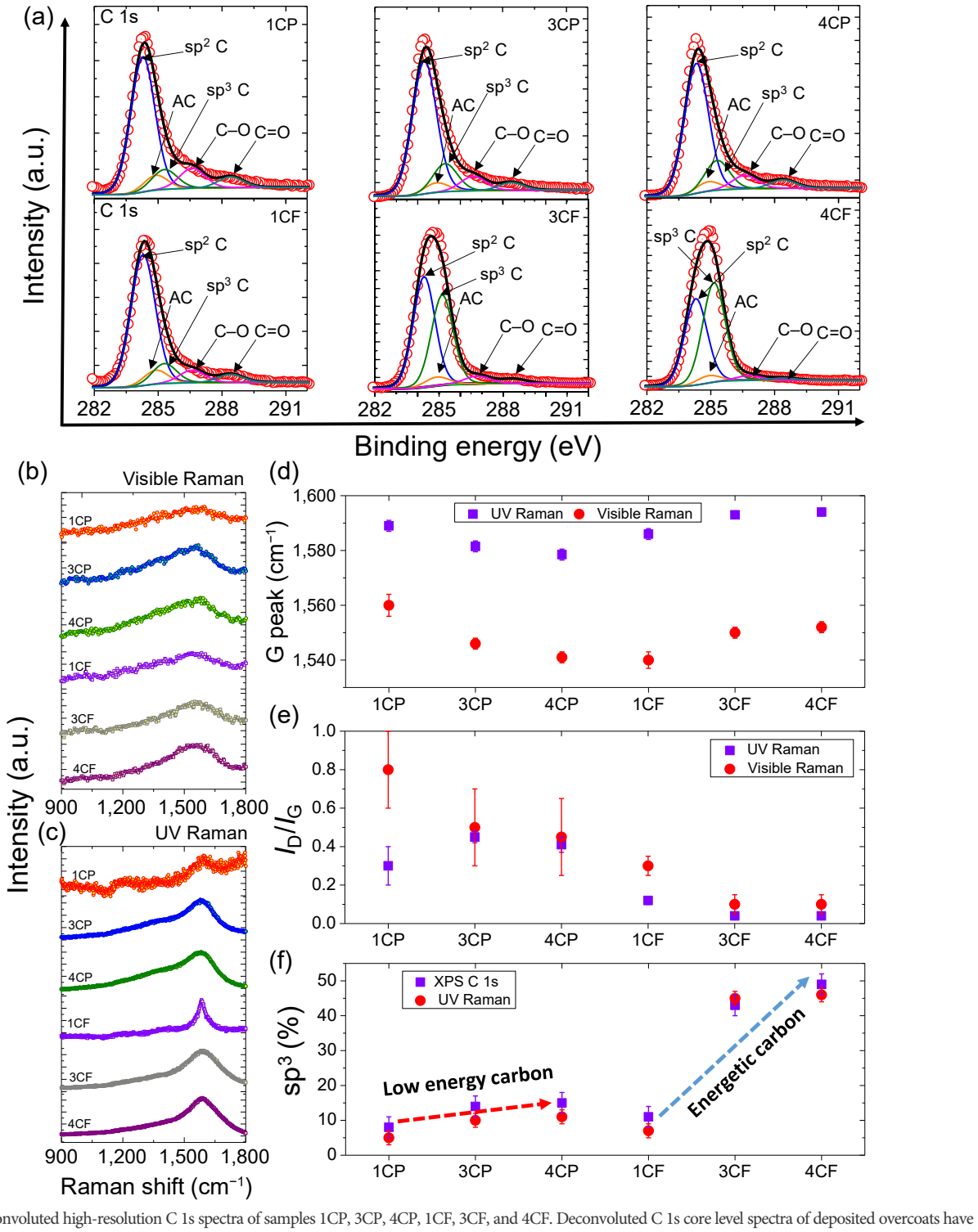

Fig. 4 (a) Deconvoluted high-resolution C 1s spectra of samples 1CP, 3CP, 4CP, 1CF, 3CF, and 4CF. Deconvoluted C 1s core level spectra of deposited overcoats have four constituent peaks corresponding to sp^2 C bonding, sp^3 C bonding, C–O bonding, and C=O bonding for all samples. An additional adventitious carbon peak was also detected. This peak is attributed to the presence of environmental organic carbon, which is typically found in all samples. (b) visible Raman and (c) UV Raman spectra. Variations in (d) G peak position, (e) I_D/I_G ratio, and (f) sp^3 C bonding content based on Raman and XPS results. In these Raman spectra, a Breit–Wigner–Fano (BWF) function was employed for fitting of G peak, whereas a Lorentzian function was employed for fitting of D peak.

overcoats of sub-5 nm thickness grown on Al_2O_3+TiC (AlTiC) substrates by energetic carbon ions/atoms, particularly at a thickness of 4 nm (i.e., sample 4CF), exhibit exceptional control of friction and wear resistance. To elucidate the reasons behind their excellent tribological performance within this thickness range, we fabricated a few different series of sub-10 nm monolithic and hybrid carbon overcoat samples using alternative deposition techniques, including pulsed DC sputtering, RF sputtering and spin-coating of multilayer graphene from solution. To understand the friction and wear control mechanisms in sample 4CF, we conducted X-ray photoelectron spectroscopy (XPS) and Raman spectroscopy measurements. The high atomic mixing and sp^3 bonding content in 4CF, coupled with a negligible I_D/I_G ratio, led to a densified carbon network that promoted the wear resistance

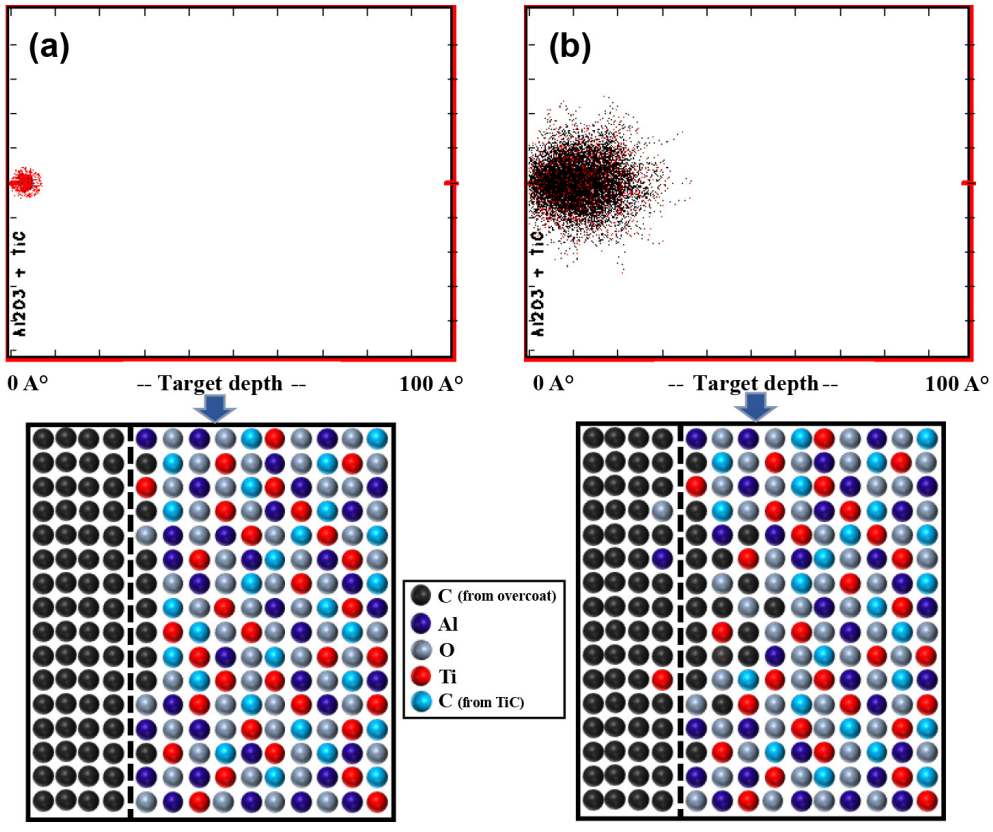

Fig. 5 TRIM simulations for atomic interaction and distribution resulting from surface bombardment by (a) low-energy species of carbon (at 4 eV) and (b) relatively high-energy species of carbon (at 90 eV); corresponding ball models illustrate different extents of intermixing of carbon atoms with AlTiC substrate in both cases.

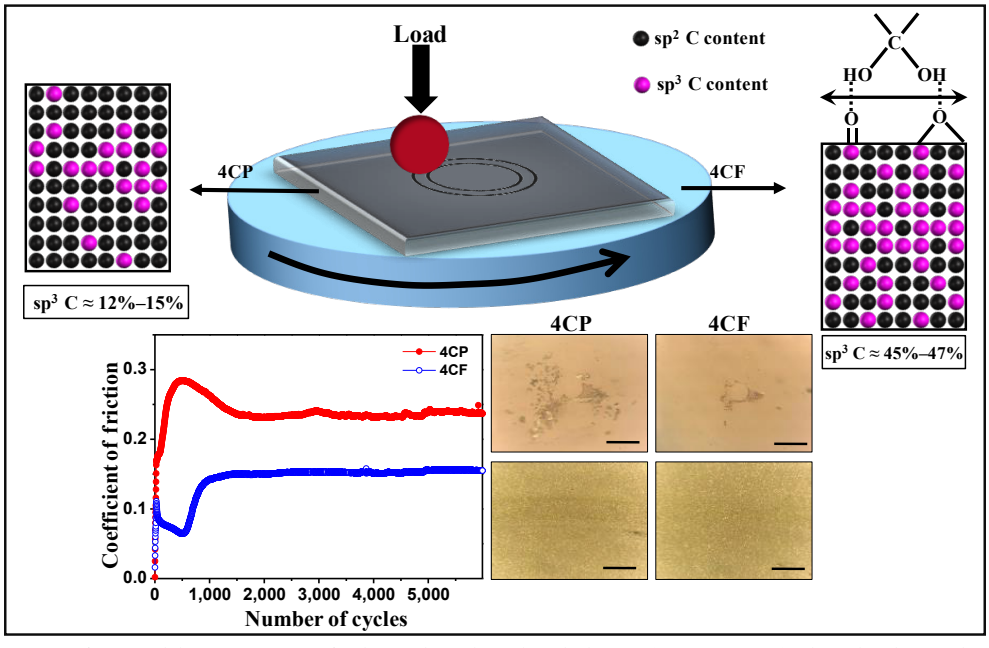

Fig. 6 Schematic illustration of contact sliding on two types of carbon with similar carbon thicknesses (4CP versus 4CF). The carbon layer with 40%–50% sp^3 bonding and more atomic mixing, illustrated by the quantity and distribution of purple and black balls, yields superior friction and wear control efficacy than the carbon layer with less sp^3 bonding and atomic mixing, as shown by frictional curves and optical microscope images of the ball (top) and wear track (bottom) after ball-on-disk tribological tests. Scale bars in optical microscope images represent 100 μm.

and low friction of the overcoat, outperforming the monolithic and hybrid overcoats grown by pulsed DC and RF sputtering techniques. The densified carbon network, in combination with significant atomic mixing generated during the energetic deposition process, was the dominant factor controlling the friction and wear of ultrathin carbon overcoats at rough tribological contacts rather than the overall overcoat thickness. Nevertheless, the addition of multilayer graphene as an overlayer to the CF overcoats, especially at 3–4 nm CF thicknesses, helped reduce the friction due to the low shear strength of the sp^2-bonded multilayer graphene, which facilitated the ease of sliding. These findings show that even at extremely low thicknesses of sub-5 nm,

ultrathin carbon overcoats grown by energetic processes can still effectively moderate the friction and wear on rough AlTiC and ceramic surfaces. This would be beneficial not only for advancing the data storage capacity in future magnetic data storage systems but also for improving the friction and wear durability of components in high-precision nano-/micro-mechanical systems containing small sliding contacts.

Acknowledgements

The authors are grateful to the Director of CSIR-AMPRI, Bhopal, India, for his kind support. This research was supported by the Department of Science and Technology (DST), India, through DST/TDT/AM/2022/253 project. Rajesh Kumar acknowledges the DST, India, for providing financial support through the DST INSPIRE Fellowship (IF200509).

Declaration of competing interest

The authors have no competing interests to declare that are relevant to the content of this article.

Electronic Supplementary Material

Supplementary material is available in the online version of this article at https://doi.org/10.26599/FRICT.2025.9441061.

References

[1] Berman D, Deshmukh S A, Sankaranarayanan S K R S, Erdemir A, Sumant A V. Macroscale superlubricity enabled by graphene nanoscroll formation. *Science* **348**(6239): 1118–1122 (2015)

[2] Erdemir A, Ramirez G, Eryilmaz O L, Narayanan B, Liao Y F, Kamath G, Sankaranarayanan S K R S. Carbon-based tribofilms from lubricating oils. *Nature* **536**(7614): 67–71 (2016)

[3] Berman D, Erdemir A, Sumant A V. Graphene: A new emerging lubricant. *Mater Today* **17**(1): 31–42 (2014)

[4] Berman D, Erdemir A, Sumant A V. Few layer graphene to reduce wear and friction on sliding steel surfaces. *Carbon* **54**: 454–459 (2013)

[5] Dwivedi N, Patra T, Lee J B, Yeo R J, Srinivasan S, Dutta T, Sasikumar K, Dhand C, Tripathy S, Saifullah M S M, et al. Slippery and wear-resistant surfaces enabled by interface engineered graphene. *Nano Lett* **20**(2): 905–917 (2020)

[6] Berman D, Erdemir A, Sumant A V. Reduced wear and friction enabled by graphene layers on sliding steel surfaces in dry nitrogen. *Carbon* **59**: 167–175 (2013)

[7] Holmberg K, Andersson P, Erdemir A. Global energy consumption due to friction in passenger cars. *Tribol Int* **47**: 221–234 (2012)

[8] Holmberg K, Erdemir A. Influence of tribology on global energy consumption, costs and emissions. *Friction* **5**(3): 263–284 (2017)

[9] Bharti P, Sunkara S V, Vishwakarma J, Jaiswal S, Dhand C, Kumar R, Kumar P, Sankaranarayanan S K R S, Dwivedi N. Simultaneous control of sliding contact and oxidation *via* graphene-based materials. *ACS Appl Eng Mater* **1**(8): 2062–2074 (2023)

[10] Bhushan B. Tribology on the macroscale to nanoscale of microelectromechanical system materials: A review. *P I Mech Eng J—J Eng* **215**(1): 1–18 (2001)

[11] Bhushan B. Micro/nanotribology of MEMS/NEMS materials and devices. In: *Springer Handbook of Nanotechnology*. Berlin (Germany): Springer, 2004: 983–1021.

[12] Kim S H, Asay D B, Dugger M T. Nanotribology and mems. *Nano Today* **2**(5): 22–29 (2007)

[13] Kumar R, Bharti P, Sasikumar K, Dhand C, Kumar R, Kumar P, Sankaranarayanan S K R S, Dwivedi N. Atomic cross-talk at the interface: Enhanced lubricity and wear and corrosion resistance in sub 2 nm hybrid overcoats via strengthened interface chemistry. *Nano Lett* **22**(24): 9795–9804 (2022)

[14] Su L Z, Zhang J D, Hu Y Z, Lam E L, Li P, Ng R W, Liang D, Zheng O, Liu H, Deng Z S. Tribological and dynamic study of head disk interface at sub-1-nm clearance. *IEEE Trans Magn* **47**(1): 111–116 (2013)

[15] Wang Y, Wei X F, Tsui K L, Chow T W S. Tribological degradation of head–disk interface in hard disk drives under accelerated wear condition. *IEEE Trans Magn* **50**(3): 3301007 (2014)

[16] Dwivedi N, Yeo R J, Dhand C, Risan J, Nay R, Tripathy S, Rajauria S, Saifullah M S M, Sankaranarayanan S K R S, Yang H, et al. Boosting contact sliding and wear protection via atomic intermixing and tailoring of nanoscale interfaces. *Sci Adv* **5**(1): eaau7886 (2019)

[17] Yeo R J, Dwivedi N, Zhang L, Zhang Z, Lim C Y H, Tripathy S, Bhatia C S. Durable ultrathin silicon nitride/carbon bilayer overcoats for magnetic heads: The role of enhanced interfacial bonding. *J Appl Phys* **117**(4): 045310 (2015)

[18] Rismani E, Yeo R, Sinha S K, Yang H, Bhatia C S. Developing an (Al, Ti)N_xC_y interlayer to improve the durability of the ta-C coating on magnetic recording heads. *Tribol Lett* **50**(2): 233–243 (2013)

[19] Bhushan B, Lowry J A. Friction and wear studies of various head materials and magnetic tapes in a linear mode accelerated test using a new nano-scratch wear measurement technique. *Wear* **190**(1): 1–15 (1995)

[20] Berman D, Erdemir A, Zinovev A V, Sumant A V. Nanoscale friction properties of graphene and graphene oxide. *Diam Relat Mater* **54**: 91–96 (2015)

[21] Strahlendorff T, Dai G L, Bergmann D, Tutsch R. Tip wear and tip breakage in high-speed atomic force microscopes. *Ultramicroscopy* **201**: 28–37 (2019)

[22] Liu J J, Notbohm J K, Carpick R W, Turner K T. Method for characterizing nanoscale wear of atomic force microscope tips. *ACS Nano* **4**(7): 3763–3772 (2010)

[23] Yang P, Liao N B. Surface sliding simulation in micro-gear train for adhesion problem and tribology design by using molecular dynamics model. *Comput Mater Sci* **38**(4): 678–684 (2007)

[24] Morales-Espejel G E, Gabelli A. A model for gear life with surface and subsurface survival: Tribological effects. *Wear* **404**: 133–142 (2018)

[25] Oh C Y, Hwang J, Jhe W. High quality factor tuning fork resonators with various resonance frequencies. *J Korean Phys Soc* **82**(4): 411–419 (2023)

[26] Katayama K, Chinda Y, Shimizu O, Goto Y, Suzuki M, Noguchi H. Long term stabilities of magnetic tape for data storage in office environment. *J Appl Phys* **117**(17): 17E305 (2015)

[27] Shimizu O, Murata Y, Kurihashi Y, Harasawa T, Asai M, Sueki M, Noguchi H. Long-term archival stability of barium ferrite magnetic tape. *J Magn Soc Jpn* **36**(1_1): 1–4 (2012)

[28] Ahmad Bhat W. Long-term preservation of big data: Prospects of current storage technologies in digital libraries. *Libr Hi Tech* **36**(3): 539–555 (2018)

[29] Bhushan B. Current status and outlook of magnetic data storage devices. *Microsyst Technol* **29**(11): 1529–1546 (2023)

[30] Lantz M. Why the future of data storage is (still) magnetic tape. IEEE Spectr Technol Eng. Sci News, 2018. Available at https://spectrum.ieee.org/why-the-future-of-data-storage-is-still-magnetic-tape

[31] Sourty E, Wild M, Sullivan J L. Pole tip recession and staining at the head to tape interface of linear tape recording systems. *Wear* **252**(3–4): 276–299 (2002)

[32] Scott W W, Bhushan B. Micro/nano-scale differential wear of multiphase materials: Pole tip recession in magnetic-tape heads. *Wear* **252**(1–2): 103–122 (2002)

[33] Luk A, Bhushan B. Durability and failure mechanisms of digital tapes in a rotary tape drive. *P I Mech Eng J—J Eng* **215**(1): 77–102 (2001)

[34] Holmberg K, Matthews A, Ronkainen H. Coatings tribology: Contact mechanisms and surface design. *Tribol Int* **31**(1–3): 107–120 (1998)
[35] Vardhan H, Singh S, Gupta S, Sharma K, Jafri Y, Gupta M, Reddy V R, Rawat R S, Gupta A, Gome A, et al. Tailoring structural and magnetic *viz*. static and dynamic properties of soft magnetic CoFeB film with Ta incorporation. *J Alloys Compd* **923**: 166357 (2022)
[36] Sourty E, Sullivan J L, Bijker M D. Chromium oxide coatings applied to magnetic tape heads for improved wear resistance. *Tribol Int* **36**(4–6): 389–396 (2003)
[37] Bernhard P, Ziethen C, Ohr R, Hilgers H, Schönhense G. Investigations of the corrosion protection of ultrathin a-C and a-C: N overcoats for magnetic storage devices. *Surf Coat Tech* **180**: 621–626 (2004)
[38] Matlak J, Rismaniyazdi E, Komvopoulos K. Nanostructure, structural stability, and diffusion characteristics of layered coatings for heat-assisted magnetic recording head media. *Sci Rep* **8**: 9807 (2018)
[39] Ebrahimi S, Steigmann D, Komvopoulos K. Peridynamics analysis of the nanoscale friction and wear properties of amorphous carbon thin films. *J Mech Mater Struct* **10**(5): 559–572 (2015)
[40] Mangolini F, Krick B A, Jacobs T D B, Khanal S R, Streller F, McClimon J B, Hilbert J, Prasad S V, Scharf T W, Ohlhausen J A, et al. Effect of silicon and oxygen dopants on the stability of hydrogenated amorphous carbon under harsh environmental conditions. *Carbon* **130**: 127–136 (2018)
[41] Rismani E, Yeo R, Mirabolghasemi H, Kwek W M, Yang H, Bhatia C S. An ultrathin multilayer TiN/SiN wear resistant coating for advanced magnetic tape drive heads. *Thin Solid Films* **556**: 354–360 (2014)
[42] Dwivedi N, Yeo R J, Zhang Z, Dhand C, Tripathy S, Bhatia C S. Direct observation of thickness and foreign interlayer driven abrupt structural transformation in ultrathin carbon and hybrid silicon nitride/carbon films. *Carbon* **115**: 701–719 (2017)
[43] Kumar R, Bharti P, Dhand C, Yeo R J, Zhang M S, Dwivedi N. "It's team work": Multilayered wear-resistant and lubricating overcoats derived from the synergy of ultrathin carbon surface and interface chemistry. *Appl Surf Sci* **641**: 158485 (2023)
[44] Bharti P, Neogi A, Sharma R, Dhand C, Kumar R, Kumar P, Sankaranarayanan S K R S, Dwivedi N. Decision trees within 1D/2D material systems for enabling highly lubricious and wear resistant surfaces. *Carbon* **217**: 118603 (2024)
[45] Ferrari A C, Robertson J. Interpretation of Raman spectra of disordered and amorphous carbon. *Phys Rev B* **61**(20): 14095–14107 (2000)
[46] Dwivedi N, Yeo R J, Zhang Z, Dhand C, Tripathy S, Bhatia C S. Interface engineering and controlling the friction and wear of ultrathin carbon films: High sp^3 versus high sp^2 carbons. *Adv Funct Mater* **26**(10): 1526–1542 (2016)
[47] Hu Z L, Fan X, Chen C. Multiscale frictional behaviors of sp^2 nanocrystallited carbon films with different ion irradiation densities. *Friction* **9**(5): 1025–1037 (2021)
[48] Konicek A R, Grierson D S, Sumant A V, Friedmann T A, Sullivan J P, Gilbert P U P A, Sawyer W G, Carpick R W. Influence of surface passivation on the friction and wear behavior of ultrananocrystalline diamond and tetrahedral amorphous carbon thin films. *Phys Rev B* **85**(15): 155448 (2012)

Rajesh Kumar is a Ph.D. scholar at CSIR-Advanced Materials and Processes Research Institute, Bhopal, India and at Academy of Scientific and Innovative Research, Ghaziabad, India. His research focuses on developing two-dimensional (2D) materials and investigation their tribological, corrosion, and structural properties for surface protection, energy, and environment applications.

Pankaj Bharti is a Ph.D. scholar at CSIR-Advanced Materials and Processes Research Institute, Bhopal, India and at Academy of Scientific and Innovative Research, Ghaziabad, India. His research focuses on developing 2D materials and investigation their tribological, corrosion and structural properties for surface protection, energy, and environment applications.

Reuben J. Yeo is a scientist at the Institute of Materials Research and Engineering (IMRE), Agency for Science, Technology and Research (A*STAR), Singapore. His research interests include surfaces and interfaces, tribology, corrosion, coatings, self-assembly, and triboelectricity.

Avanish K. Srivastava is a distinguished scientist and currently serves as the Director of the CSIR-Advanced Materials and Processes Research Institute, Bhopal, India. Dr. Srivastava has contributed significantly in the field of processing, characterization, properties, and possible applications of metals and alloys, composites, semiconductors, and various nanostructures.

Chetna Dhand is a senior scientist at CSIR-Advanced Materials and Processes Research Institute, Bhopal, India, and assistant professor at Academy of Scientific and Innovative Research, Ghaziabad, India. Her major research interests include nano-biomaterials, electrochemical sensors/biosensors, 2D materials, bio-inspired catecholamine chemistry, antimicrobial materials and coatings, advanced wound care materials, etc.

Neeraj Dwivedi is a principal scientist at CSIR-Advanced Materials and Processes Research Institute, Bhopal, India, and associate professor at Academy of Scientific and Innovative Research, Ghaziabad, India. His research interest includes interface engineering, carbon nanocoatings, 2D materials such as graphene-based materials, MXenes, metal oxides, and nitrides for tribological, corrosion, energy, sensing, and antimicrobial applications.